

Viscous dissipation and chemical reaction effects on MHD Casson nanofluid over a stretching sheet

Kamatam Govardhan ^a, Ganji Narender ^{b, *}, Gobburu Sreedhar Sarma ^b

^a Department of Mathematics, GITAM University Hyderabad-502329, Telangana State, India

^b Department of Humanities & Science, CVR College of Engineering, Hyderabad-501510, Telangana State, India

* Corresponding author: gnriimc@gmail.com

Article history

Received 5 May 2018
 Revised 1 June 2018
 Accepted 2 July 2018
 Published Online 25 August 2019

Abstract

A numerical analysis was performed for the mathematical model of boundary layer flow of Casson nanofluids. Heat and mass transfer were analyzed for an incompressible electrically conducting fluid with viscous dissipations and chemical reaction past a stretching sheet. An appropriate set of similarity transformations were used to transform the governing partial differential equations (PDEs) into a system of nonlinear ordinary differential equations (ODEs). The resulting system of ODEs is solved numerically by using shooting method. A detailed discussion on the effects of various physical parameters and heat transfer characteristics was also included.

Keywords: Chemical reaction, viscous dissipation, magnetohydrodynamic, stagnation point, nanofluids

© 2019 Penerbit UTM Press. All rights reserved

INTRODUCTION

Nanofluid technology has been receiving a lot of attention as a research topic and takes important part for further development of higher performance due to effective applications in the field of electronics engineering, transportation, and biomedical research. Nanofluid refers to the suspension of nano sized particles (1-100 nm diameters) in base fluids. It has a higher thermal conductivity that shows significant enhancement due to the rate of heat transfer in industrial applications. The cooling applications of nanofluids show the importance on itself and increased attention worldwide. The applications of this technology include electronics device cooling, transformer cooling, vehicles cooling, silicon mirror cooling, and controlling fusion. There are numerous biomedical applications that involve nanofluids such as magnetic cell separation, drug delivery, cancer therapeutics, cryopreservation, and nanocryosurgery. Currently, it has been an ongoing topic of discussion as coolant for computers, safe coolant for nuclear reactors, and in a public health practice.

Carragher and Crane [1] investigated the heat transfer in the flow over a stretching surface, in the case when the temperature difference between the surface and the ambient fluid is proportional to a power of distance from the fixed point. An unsteady flow past a stretching sheet was studied by Na and Pop [2]. The radiation effect is now an attractive topic and several researchers have been done on thermal radiation. Pop et al. [3] determined the flow over stretching sheet near a stagnation point taking the effect of thermal radiation.

The research on nanofluids is gaining a lot of attention in recent few years. The effect of various parameters on nanofluid thermal conductivity has been obtained by Jang and Choi [4]. The convective heat transfer in a nanofluid past a vertical plate using a model in which Brownian motion and thermophoresis are accounted with the simplest possible boundary conditions have been discussed by Kuznetsov and Nield [5, 6]. They also studied the problem of natural convection past a vertical plate analytically in a porous medium saturated by a nanofluid [5, 6]. Khan and Pop [7] have investigated the problem of laminar fluid flow over the stretching surface in a nanofluid and they investigated it

numerically. Ibrahim and Shanker [8] analyzed MHD boundary layer flow and heat transfer of a nanofluid past a permeable stretching sheet with velocity, thermal, and slip boundary conditions.

In the context of heat transfer process, viscous dissipations mean heating up the fluid via different source. In short, in this mechanism the viscosity of the fluid will absorb heat from the kinetic energy and transform it into internal energy of the system. Moreover, the process in which the electric current through a conductor produce heat is known as Joule heating. Eldahab et al. [9] studied the viscous dissipation and Joule heating effects on MHD-free convection from a vertical plate. Viscous dissipations play an important role in the natural convection in various devices. Viscous dissipation effects and the effects of Joule heating on thermal boundary layer flow are studied in [10, 11]. Aminreza et al. [12] examined the effect of partial slip on flow and heat transfer of nanofluids past a stretching sheet.

Hence the objective of this study was to review a study of Wubshet Ibrahim et al. [13] and extend the flow analysis by considering the additional effects of nanofluid, viscous dissipation, and nonlinear thermal radiation with the assumptions of laminar, steady, incompressible, two-dimensional, porous stretching sheet, nanofluid with elector-hydrodynamic, convective boundary condition, and micro-slip condition on the wall. The obtained system of PDEs was transformed into a system of non-linear and coupled ODEs by using a suitable similarity transformation. A numerical solution of the system of ODEs was obtained by employing the shooting method and the precision of the obtained numerical results was compared by using the Matlab bvp4c function. The mathematical inferences were discussed for different physical parameters appearing in the solution influencing the flow and heat transform.

MATHEMATICAL MODEL OF THE FLOW

Consider the numerical investigation of MHD boundary layer flow of an incompressible Casson nanofluid, the cartesian coordinates x , measured along the stretching surface and y is the coordinate measured

normal to the stretching surface. The physical configuration and coordinate system are shown in Fig 1. Initially it is assumed that fluid and the plate are at rest after that the plate is moved with a constant velocity $u = u_w = ax$ and $u_\infty = bx$, (where a and b are positive constants) along x -direction. In addition, fluid is flowing in the presence of magnetic field. The magnetic field is supposed to be applied along the y -direction. The slip velocity at the surface is $U_{slip} = (\mu_B + \frac{p_y}{\sqrt{2\pi_c}}) \frac{\partial u}{\partial y}$. Two equal and opposite forces are applied along the x -axis, so that the sheet is stretched keeping the origin fixed.

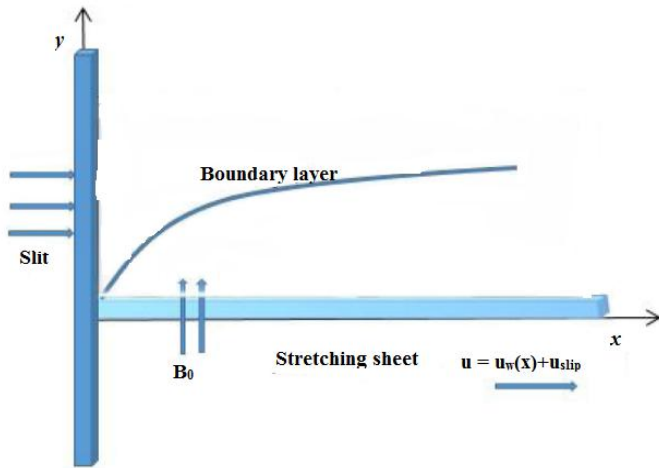


Figure 1 Geometry for the flow under consideration.

The rheological equation of state for an isotropic and incompressible flow of a Casson fluid can be written as follows:

$$\tau^{1/2} = \tau_0^{1/2} + \mu\gamma^{1/2} \tag{1}$$

$$\tau_{ij} = \begin{cases} 2\left(\mu_B + \frac{p_y}{\sqrt{2\pi}}\right) e_{ij}, & \pi > \pi_c \\ 2\left(\mu_B + \frac{p_y}{\sqrt{2\pi_c}}\right) e_{ij}, & \pi_c > \pi \end{cases} \tag{2}$$

where μ_B is the plastic dynamic viscosity of the non-Newtonian fluid, p_y is the yield stress of fluid, π is the product of the component of deformation rate and itself, namely, $\pi = e_{ij}e_{ij}$, e_{ij} is the (i, j) component of the deformation rate, and π_c is a critical value of π based on non-Newtonian model. The equation of continuity, equation of momentum and the energy equation describing the given two dimensional flows.

The Continuity equation

$$\frac{\partial u}{\partial x} + \frac{\partial v}{\partial y} = 0 \tag{3}$$

The Momentum equation

$$u \frac{\partial u}{\partial x} + v \frac{\partial u}{\partial y} = U_\infty \frac{\partial U_\infty}{\partial x} + \frac{\sigma B_0^2(x)}{\rho_f} (U_\infty - u) + \nu \left(1 + \frac{1}{\gamma}\right) \frac{\partial^2 u}{\partial y^2} \tag{4}$$

The Energy equation

$$u \frac{\partial T}{\partial x} + v \frac{\partial T}{\partial y} = \frac{\mu}{c_p} \left(1 + \frac{1}{\gamma}\right) \left(\frac{\partial u}{\partial y}\right)^2 + \alpha \frac{\partial^2 T}{\partial y^2} + \Gamma \left[D_B \frac{\partial c}{\partial y} \frac{\partial T}{\partial y} + \frac{D_T}{T_\infty} \left(\frac{\partial T}{\partial y}\right)^2 \right] \tag{5}$$

The Concentration equation

$$\frac{\partial c}{\partial x} + v \frac{\partial c}{\partial y} = D_B \frac{\partial^2 c}{\partial y^2} + \frac{D_T}{T_\infty} \frac{\partial^2 c}{\partial y^2} - k_0 (C - C_\infty) \tag{6}$$

The initial and boundary conditions are:

$$\begin{aligned} u &= U_w(x) + U_{slip} \Rightarrow u = ax + \left(\mu_B + \frac{p_y}{\sqrt{2\pi_c}}\right) \frac{\partial u}{\partial y}, v = 0, \\ -k \frac{\partial T}{\partial y} &= h(T_f - T), C = C_w \text{ at } y = 0 \\ u \rightarrow U_\infty &= bx, v = 0, T \rightarrow T_\infty, C \rightarrow C_\infty \text{ as } y = \infty \end{aligned} \tag{7}$$

where $\gamma = \mu_B \sqrt{2\pi_c} / p_y$ is the Casson parameter, $\nu = \mu_B / \rho$ is the kinematics viscosity, α is the thermal diffusivity, k is the thermal conductivity, D_B is the Brownian diffusion coefficient, D_T is the thermophoresis diffusion coefficient, where, x is the coordinate measured along stretching surface, U_w is the stretching velocity and U is the uniform velocity. Now we convert the system of Eqs. (3) - (6) following the boundary conditions into a unitless form. For this purpose, we use the following similarity transformation.

$$\eta = y \sqrt{\frac{a}{\nu}}, \psi = \sqrt{a\nu x} f(\eta), \theta(\eta) = \frac{T - T_\infty}{T_f - T_\infty}, \beta(\eta) = \frac{C - C_\infty}{C_w - C_\infty} \tag{8}$$

The continuity Eq. (3) is identically satisfied for the stream function $\psi(x, y)$. The velocity components are given by:

$$u = \frac{\partial \psi}{\partial y}, v = -\frac{\partial \psi}{\partial x} \tag{9}$$

Using the similarity transformation from Eq. (8) in momentum Eq. (4), energy Eq. (5) and concentration Eq. (6) along the boundary conditions (7) we get the following system of ODEs:

$$\left(1 + \frac{1}{\gamma}\right) f''' + ff'' - (f')^2 + M(A - f') + A^2 = 0 \tag{10}$$

$$\theta'' + Prf\theta' + PrNb\theta'\beta' + PrNt(\theta')^2 + \left(1 + \frac{1}{\gamma}\right) PrEc(f'')^2 = 0 \tag{11}$$

$$\beta'' + Lef\beta' + \frac{Nt}{Nb}\theta'' - Le\chi\beta = 0 \tag{12}$$

Here $f(\eta), \theta(\eta)$ and $\beta(\eta)$ are function of η and prime denotes derivative w.r.t η . The transformed BCs in the modeled problem are:

$$\left. \begin{aligned} f(0) &= 0, f'(0) = 1 + \delta \left(1 + \frac{1}{\gamma}\right) f''(0), \\ \theta'(0) &= -Bi[1 - \theta(0)], \beta(0) = 1, \text{ at } \eta = 0, \\ f'(\infty) &\rightarrow A, \theta(\infty) \rightarrow 0, \beta(\infty) \rightarrow 0 \text{ as } \eta \rightarrow \infty \end{aligned} \right\} \tag{13}$$

The associated parameters appearing in the modeled problem are:

$$\begin{aligned} Pr &= \nu/\alpha, Le = \alpha/D_B, M = \sigma B_0^2/\rho_f a, Nb = \rho_p D_B (C_w - C_\infty)/\rho_f \alpha, \\ Nt &= \rho_p D_T (T_w - T_\infty)/\rho_f \alpha T_\infty, A = b/a, \delta = \mu_B \sqrt{a/\nu}, Bi = \frac{hf}{k} \sqrt{\frac{\nu}{a}}, \\ Ec &= u_w^2/\rho_f (T_w - T_\infty), \chi = \mathcal{K}_0/b. \end{aligned}$$

Pr denotes the Prandtl number, Le is the Lewis number, M is a magnetic parameter, Nb is the Brownian motion parameter, Nt the thermophoresis parameter, A is velocity ratio parameter, δ is the thermal slip parameter, Bi the Biot member, Ec is the Eckert number and χ is the chemical reaction parameter. It should be mentioned here that $(\chi > 0)$ indicates a destructive chemical reaction while $(\chi < 0)$ corresponds to a generative chemical reaction.

The quantities of practical interest in this study are the Nusselt number Nu_x , the skin friction coefficient C_f , and the Sherwood number Sh_x , respectively.

$$C_f = \frac{\tau_w}{\rho u_w^2}, Nu_x = \frac{xq_w}{k(T_w - T_\infty)}, Sh_x = \frac{xh_m}{D_B(C_w - C_\infty)} \tag{14}$$

where τ_w is the shear stress along the stretching surface, q_w is the heat flux from the stretching surface, and h_w is the wall mass flux, which are given by

$$\tau_w = \left(\mu_B + \frac{p_y}{\sqrt{2\pi c}} \right) \left(\frac{\partial u}{\partial y} \right)_{y=0}, q_w = -k \left(\frac{\partial T}{\partial y} \right)_{y=0}, h_m = -D_B \left(\frac{\partial C}{\partial y} \right)_{y=0} \quad y'_6 = y_7 \quad y_6(0) = 1 \quad (22)$$

$$(15) \quad y'_7 = -Le y_1 y_7 - \frac{Nt}{Nb} y'_5 + Le \chi y_6 \quad y_7(0) = Y_7 \quad (23)$$

Using the dimensionless variables, we get

$$C_f \sqrt{R_x} = \delta \left(1 + \frac{1}{\gamma} \right) f''(0), \quad \frac{Nu_x}{\sqrt{R_x}} = -\theta'(0), \quad \frac{Sh_x}{\sqrt{R_x}} = -\beta'(0) \quad (16)$$

where $R_x = U_w(x/\nu)$ is the local Reynolds number based on stretching velocity u .

SOLUTION METHODOLOGY

The analytical solution of the system of Eqs. (10) – (12) together with boundary conditions (13) cannot be found because they are coupled and nonlinear in nature. These nonlinear coupled ODEs are solved numerically by the shooting technique with Adams – Moulton method. To apply this technique, we first convert the system of ODEs of higher order into the system of ODEs of first order. Eqs. (10) – (12) can be rewritten as follows:

$$f''' = \frac{-(f f'' - (f')^2 + M(A - f') + A^2)}{\left(1 + \frac{1}{\gamma}\right)}$$

$$\theta'' = -Pr \left[f \theta' + Nb \theta' \beta' + Nt(\theta')^2 + \left(1 + \frac{1}{\gamma}\right) Ec (f'')^2 \right]$$

$$\beta'' = -Le f \beta' - \frac{Nt}{Nb} \theta'' + Le \chi \beta = 0$$

By using the following notations,

$$f = y_1, f' = y_2, f'' = y_3, \theta = y_4, \theta' = y_5, \beta = y_6, \beta' = y_7$$

the system of first order ODEs are:

$$y'_1 = y_2, \quad y_1(0) = 0 \quad (17)$$

$$y'_2 = y_3, \quad y_2(0) = 1 + \delta \left(1 + \frac{1}{\gamma} \right) Y_3 \quad (18)$$

$$y'_3 = \frac{-(y_1 y_3 - (y_2)^2 + M(A - y_2) + A^2)}{\left(1 + \frac{1}{\gamma}\right)} \quad y_3(0) = Y_3 \quad (19)$$

$$y'_4 = y_5 \quad y_4(0) = Y_4 \quad (20)$$

$$y'_5 = -Pr \left(y_1 y_5 + Nb y_5 y_7 + Nt y_5^2 + \left(1 + \frac{1}{\gamma} \right) Ec y_3^2 \right) \quad y_5(0) = Bi(Y_4 - 1) \quad (21)$$

To solve the system of equations shown, the unbounded domain $[0, \eta_\infty]$ is restricted to a bounded domain $[0, \eta_e]$, where $\eta_e = 6$. This is due to the fact that increasing the value of η_e beyond 6 gives negligible variation in the numerical results. In the modeled problem, $Y_3, Y_4,$ and Y_7 are initial guesses which are required to solve the above first order system of ordinary differential equations with fourth order Adams-Moulton method. Newton iterative scheme is used to refine those initial guesses. The iterative process is repeated until the following criteria is met.

$$\max(|y_2(\eta_\infty)|, |y_4(\eta_\infty)|, |y_6(\eta_\infty)|) < \epsilon,$$

where $\epsilon = 10^{-5}$ is the tolerance for the modeled problem.

CODE VALIDATION

In Table 1, comparison of Skin Friction Coefficient $-f''(0)$ for different values of δ is displayed. The obtained results were compared of results with those obtained by Andersson [14], Hayat et al. [15], and Ibrahim et al. [8]. The results of this study were in excellent agreement with the previous works. From Table 1, it is observed that in friction coefficient is decreased by increasing the slip parameter.

Table 2 shows that the skin-friction coefficient $-f''(0)$ decreases by the increase of A . The effect of δ on Nusselt number $-\theta'(0)$ decreases and Sherwood number $-\beta'(0)$ is the opposite of the Nusselt number.

Table 3 presents the local Nusselt number and local Sherwood number for different values of thermophoresis parameter Nt , Brownian motion parameter Nb , and Biot number Bi . It is observed that when Nt increases, both the local Nusselt number and local Sherwood number increases. When Nb increases, both the values of local Sherwood number and the local Nusselt number decreases. When Bi increases, the local Nusselt number increases and local Sherwood number decreases.

Table 4 shows the numerical values $\left(1 + \frac{1}{\gamma}\right) f''(0), \theta'(0),$ and $\beta'(0)$. It is observed that the friction factor and the heat and mass transfer rates reduce with an increase in the slip parameter. When Casson parameter γ increases, the magnitude of the friction factor and the mass transfer rate diminish. For the case $(0.3 \leq \gamma \leq 4)$, the heat transfer rate is enhanced, whereas the opposite results hold with the case $(\gamma \rightarrow \infty)$.

Table 5 shows the numerical values of rate of heat transfer and rate of mass transfer due to variation in the below stated parameters.

Table 1. Comparison of Skin Friction Coefficient $f''(0)$ for different values of slip parameter δ when $M = A = 0, Bi = 10,000,$ and $\gamma = 1,000$.

δ	Andersson [14]	Hayat et al. [15]	Ibrahim and Shanker [8]	Wubshet Ibrahim and Makinde [13]	Present results
0.0	1.0000	1.000000	1.0000	1.0000	0.9999855
0.1	0.8721	0.872082	0.8721	0.8721	0.8720812
0.2	0.7764	0.776377	0.7764	0.7764	0.7763964
0.5	0.5912	0.591195	0.5912	0.5912	0.5912748
2.0	0.2840	0.283981	0.2840	0.2840	0.2841796
5.0	0.1448	0.144841	0.1448	0.1448	0.1450588
10.0	0.0812	0.081249	0.0812	0.0812	0.0814330
20.0	0.0438	0.043782	0.0438	0.0438	0.0439329
50.0	0.0186	0.018634	0.0186	0.0186	0.0186789

Table 2. Comparison of Skin Friction Coefficient $-f''(0)$, local Nusselt number $-\theta'(0)$, and local Sherwood number $-\phi'(0)$ for different values of δ , γ , and A when $Nb = Nt = 0.1$, $Pr = Le = 10$, $Bi = 0.1$, and $M = 1$.

A	δ	γ	$-f''(0)$		$-\theta'(0)$		$-\phi'(0)$	
			[13]	Present results	[13]	Present results	[13]	Present results
0.0	0.1	10	1.1451	1.1414830	0.0922	0.0921669	2.0435	2.0434700
0.1			1.0653	1.0653210	0.0923	0.0923036	2.0849	2.0848620
0.2			0.9792	0.9791939	0.0924	0.0924430	2.1283	2.1282550
0.3			0.8838	0.88382410	0.0926	0.0925826	2.1730	2.1730430
0.9			0.1467	0.1466890	0.0934	0.0933622	2.4534	2.4533620
1.5			-0.8188	-0.8188152	0.0940	0.0940005	2.7333	2.7333010
2.0			-1.7623	-1.7622860	0.0944	0.0944359	2.9597	2.9597170
2.4			-2.5944	-2.5944010	0.0947	0.0947337	3.1356	3.1356140
0.4	0.2		0.6758	0.6757960	0.0925	0.0924937	2.1478	2.1477870
	0.4		0.5357	0.5356795	0.0921	0.0921433	2.0464	2.0464120
	0.6		0.4449	0.4449050	0.0919	0.0918827	1.9768	1.9767530
	0.8		0.3810	0.0934260	0.0917	0.0916797	1.9256	1.9255770
	0.4	0.1	0.0908	0.0907876	0.0916	0.0915679	1.9015	1.9014960
		0.5	0.2563	0.2563434	0.0920	0.0919709	2.0018	2.0018460
		1	0.3477	0.3477455	0.0921	0.0920584	2.0246	2.0245580
		10	0.5357	0.5356796	0.0921	0.0921433	2.0464	2.0464120
		100	0.5688	0.5688785	0.0921	0.0921503	2.0482	2.0481280

Table 3. Comparison of local Nusselt number $-\theta'(0)$ and local Sherwood number $-\phi'(0)$ for different values of Nt, Nb , and Bi when $Pr = 7, \gamma = 100, \delta = A = 0.4$ and $Le = 2$.

Nt	Nb	Bi	$-\theta'(0)$		$-\phi'(0)$	
			[13]	Present results	[13]	Present results
0.1	0.1	0.5	0.3621	0.3620915	0.6508	0.6508213
0.5			0.3383	0.3382888	-0.0498	-0.0497656
1.0			0.2856	0.2855649	-0.1853	-0.1852617
0.1	0.2		0.3349	0.3349248	0.7849	0.7849264
	0.5		0.2212	0.2212252	0.8732	0.8731724
	1.0		0.0467	0.0466859	0.8950	0.8949944
	0.1	0.1	0.0931	0.0931472	0.8156	0.8155568
		0.5	0.3621	0.3620915	0.6508	0.6508211
		1	0.5609	0.5608643	0.5328	0.5328193
		5	0.9680	0.9679839	0.3031	0.3030508
		10	1.0576	1.0575730	0.2550	0.2550032
		20	1.1076	1.1076510	0.2286	0.228595

Table 4: Computed values of $(1 + \frac{1}{\gamma})f''(0), \theta'(0)$, and $\beta'(0)$ with δ, Bi, A, γ for $Nb = Nt = 0.1, Ec = \chi = 0.2, Pr = 4.0$ and $Le = 5.0$.

δ	Bi	A	γ	$(1 + \frac{1}{\gamma})f''(0)$	$-\theta'(0)$	$-\beta'(0)$
0	0.2	0.2	0.5	-2.1068	0.1083879	2.0288250
1	0.2	0.2	0.5	-0.5570	0.1504452	1.4497390
3	0.2	0.2	0.5	-0.2316	0.1501755	1.3227600
0.2	0	0.2	0.5	-1.3252	0.0000000	1.7820560
0.2	1	0.2	0.5	-1.3252	0.3868136	1.6708380
0.2	3	0.2	0.5	-1.3252	0.5495870	1.6313440
0.2	0.2	0	0.5	-1.554648	0.1150509	1.7133470
0.2	0.2	1	0.5	0.000001	0.1722542	1.9661090
0.2	0.2	3	0.5	4.881635	0.0558054	3.3755600
0.2	0.2	0.2	0.3	-1.487385	0.1355280	1.7266590
0.2	0.2	0.2	4	-0.980994	0.1360230	1.7457790
0.2	0.2	0.2	∞	-0.903319	0.1362902	1.7404570

Table 5: Numerical solution of $-\theta'(0)$, and $-\beta'(0)$ with Nb, Nt, χ and Ec for $\delta = Bi = A = 0.2, \gamma = 0.2, Pr = 4.0, M = 1.0$ and $Le = 5.0$.

Nt	Nb	χ	Ec	$-\theta'(0)$	$-\beta'(0)$
0.1	0.1	0.2	0.2	0.1355178	1.7405510
0.3	0.1	0.2	0.2	0.1310324	1.8341440
0.5	0.1	0.2	0.2	0.1255335	1.9767680
0.1	0.2	0.2	0.2	0.1245157	1.7400480
0.1	0.4	0.2	0.2	0.0963147	1.7426440
0.1	0.6	0.2	0.2	0.0614046	1.7447390
0.1	0.1	-0.2	0.2	0.1365149	1.0101670
0.1	0.1	0.0	0.2	0.1359263	1.4140470
0.1	0.1	0.4	0.2	0.1352170	2.0185960
0.1	0.1	0.2	0.0	0.1654778	1.6562840
0.1	0.1	0.2	1.0	0.0086006	2.0899780
0.1	0.1	0.2	1.3	-0.0422648	2.2265390

RESULTS AND DISCUSSION

The objective of this section was to analyze the numerical results displayed in the tabular and graphical form. The numerical influence of different parameters. For instance Prandtl number (Pr), magnetic parameter (M), Brownian motion parameter (Nb), thermophoresis parameter (Nt), Lewis number (Le), Slip parameter (δ), Biot number (Bi), Eckert number (Ec), chemical reaction parameter (χ) on the velocity profile, temperature profile, and concentration profile are displayed graphically.

Impact of velocity ratio parameter

Figure 2 designates that by enlarging A ($A > 1$), the width of the hydrodynamic boundary layer increases, and vice versa. Physically, the ratio between free stream velocity and the stretching velocity is greater than 1 if stretching velocity becomes less than the free stream velocity. Consequently, flow velocity is increased when retarding force is decreased.

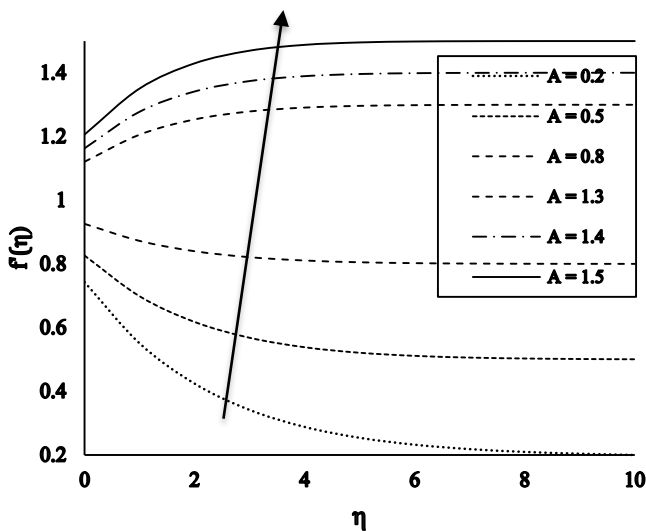


Figure 2. Velocity profile vs A when $Nb = Nt = 0.5, Le = 2, Pr = M = 1, Bi = 0.5, \gamma = 0.1, \delta = 0.2, Ec = 0.2$ and $\chi = 0.2$.

The effect of velocity ratio parameter A on the temperature profile $\theta(\eta)$ is presented in Figure 3. As we increase the value of velocity ratio parameter A , the temperature at the surface declines, and as a result, it also declines the thickness of the thermal boundary layer.

Figure 4 demonstrates the concentration vs velocity ratio. As the concentration distribution decreases by increasing the velocity ratio parameter A .

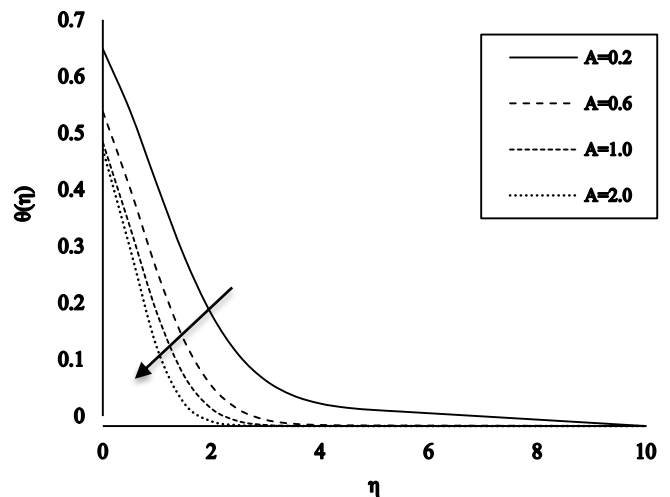


Figure 3. Temperature profile vs A when $Nb = Nt = 0.5, Le = 2, Pr = M = 1, Bi = 0.5, \gamma = 0.1, \delta = 0.2, Ec = 0.2$ and $\chi = 0.2$

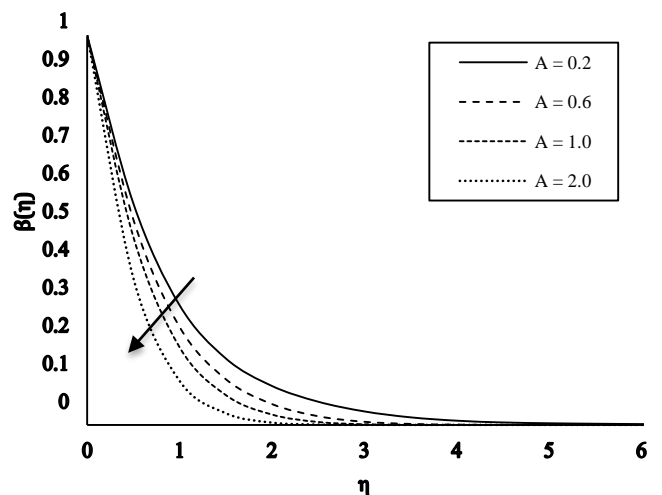


Figure 4. Concentration profile vs A when $Nb = Nt = 0.5, Le = 2, Pr = M = 1, Bi = 0.5, \gamma = 0.1, \delta = 0.2, Ec = 0.2$ and $\chi = 0.2$.

Impact of Eckert number

Figure 5 displays the influence of Eckert number Ec on concentration profile. It is observed that the concentration of the fluid increase near the plate. However, it diminishes away from the surface as the value of Eckert number is enhanced. Figure 6 shows the effect of

Eckert number Ec on the energy profile. Energy profile increases when increase Eckert number Ec .

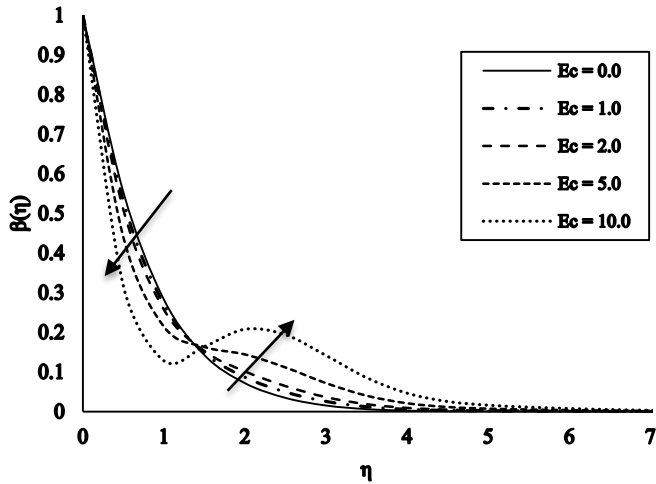


Figure 5 Concentration profile vs Ec when $Nb = Nt = 0.1, Le = 2.0, A = 0.4, Pr = 5, M = 1, Bi = 0, \gamma = 0.1, \delta = 0.2$ and $\chi = 0.2$.

cause a higher energy and increasing the thermal boundary layer thickness. Physically, convective heating Bi can be calculated by dividing the convection at the surface to the conduction on the surface of a body. The Biot number causes a decrease in the concentration profile as reflected in Figure 9.

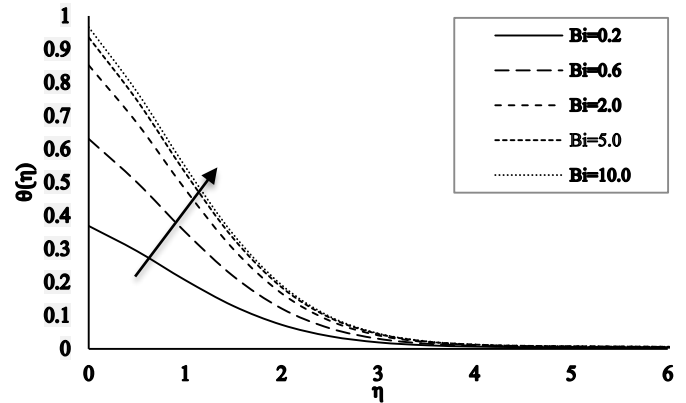


Figure 8. Temperature profile vs Bi when $Nb = Nt = 0.5, Le = 2, Pr = M = 1, \gamma = 0.1, \delta = 0.2, A = 0.4, Ec = 0.2$ and $\chi = 0.2$.

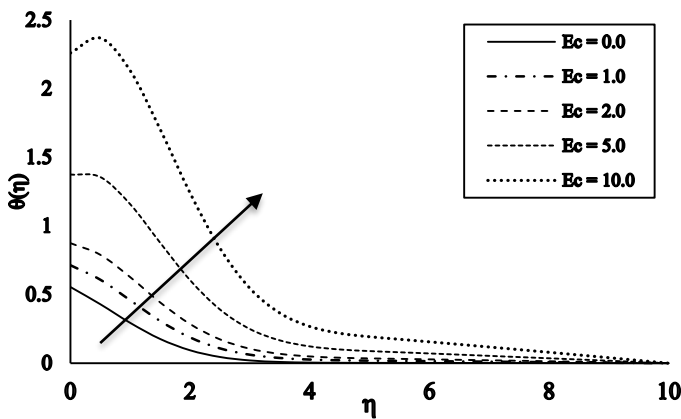


Figure 6. Temperature profile vs Ec when $Nb = Nt = 0.1, Le = 2.0, A = 0.4, Pr = 5, M = 1, Bi = 0, \gamma = 0.1, \delta = 0.2$ and $\chi = 0.2$.

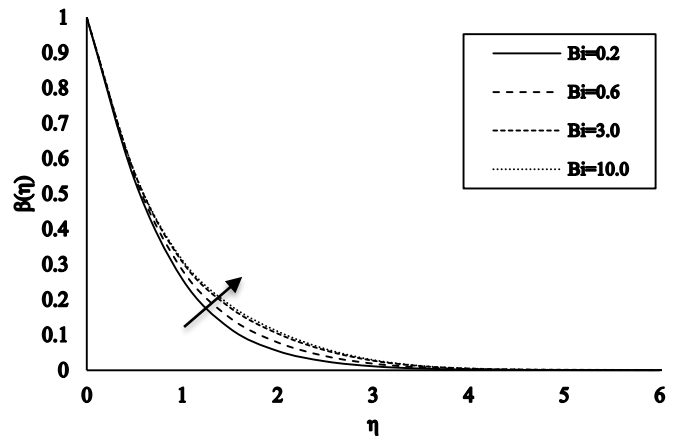


Figure 9. Concentration profile vs Bi when $Nb = Nt = 0.1, Pr = 5, M = 1, A = 0.4, \delta = 0.1, \gamma = Ec = 0.2$ and $\chi = 0.2$.

Impact of Lewis number

Figure 7 shows the influences of Lewis number Le on the concentration profile $\beta(\eta)$. The concentration profile falls when we increase the values of Lewis number Le .

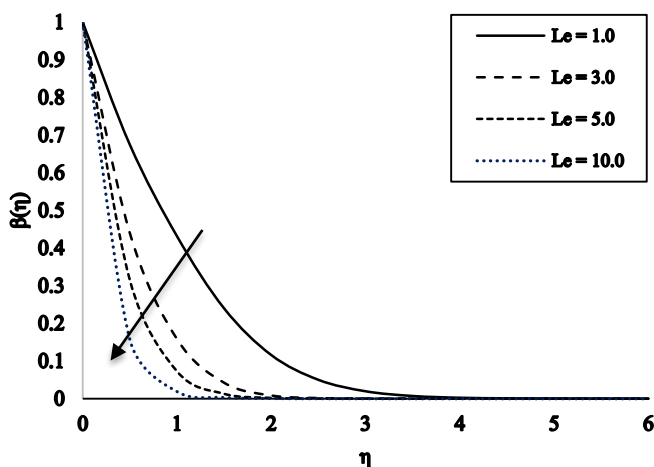


Figure 7 Concentration profile vs Le when $Nb = Nt = 0.1, A = 0.4, Pr = 5, M = 1, Bi = \gamma = 0.1, \delta = 0.2, Ec = 0.2$ and $\chi = 0.2$

Brownian motion parameter

It is noticed from Figure 10 that as the value of Nb increases, the thermal boundary layer thickens. The impact of Brownian motion parameter is witness in Figure 11 that the concentration profile increases by increasing the Nb . Consequently, the Brownian force increases the nanoparticle concentration at the surface. Thus, the concentration profile increases on the surface but it is found to decrease a bit away from the surface.

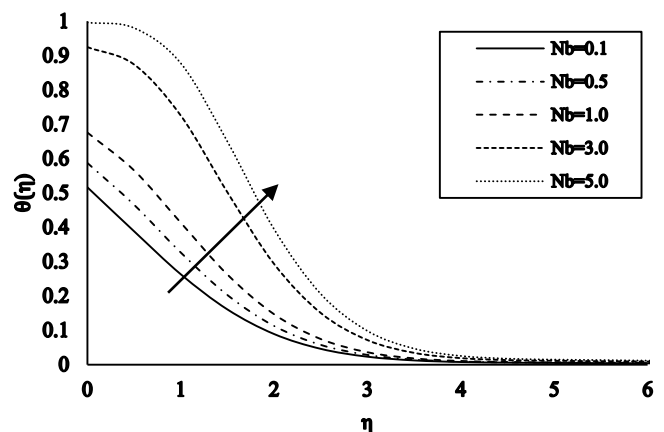


Figure 10. Temperature profile vs Nb when $Bi = 0.5, Nt = 0.5, Le = 2, Pr = M = 1, \gamma = 0.1, \delta = 0.2, A = 0.4, Ec = 0.2, \chi = 0.2$

Impact of Biot number

Figure 8 demonstrates the impact of the Biot number on the temperature $\theta(\eta)$. We notice that the enhanced values of Biot number

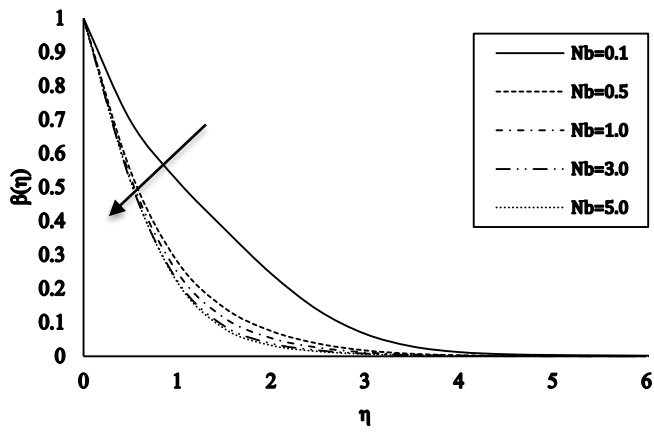


Figure. 11. Concentration profile vs Nb when $Bi = 0.5, Nt = 0.5, Le = 2, Pr = M = 1, \gamma = 0.1, \delta = 0.2, A = 0.4, Ec = 0.2, \chi = 0.2$

Thermophoresis parameter

Figure 12 includes the graphs of the temperature distribution in thermal boundary layer for various value of the Nt . It is noticed that if the thermophoresis increases, this causing an increase in Nt . Figure 13 describes the influence of the Nt on the concentration profile. Therefore, when the influence of the thermophoretic force is enlarged, the concentration profile on the surface declines, which is the opposite in nature to that of the case of the Brownian motion but it starts increasing when it is away from the wall.

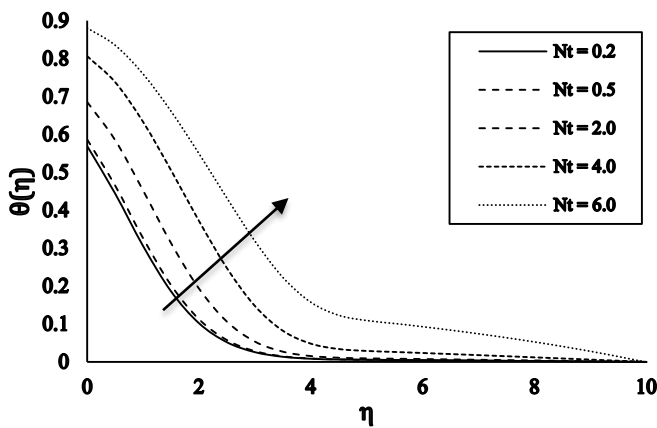


Figure. 12. Temperature profile vs Nt when $Nb = 0.5, Le = 2, Pr = M = 1, Bi = 0.5, \delta = 0.1, A = 0.4, Ec = 0.2$ and $\chi = 0.2$.

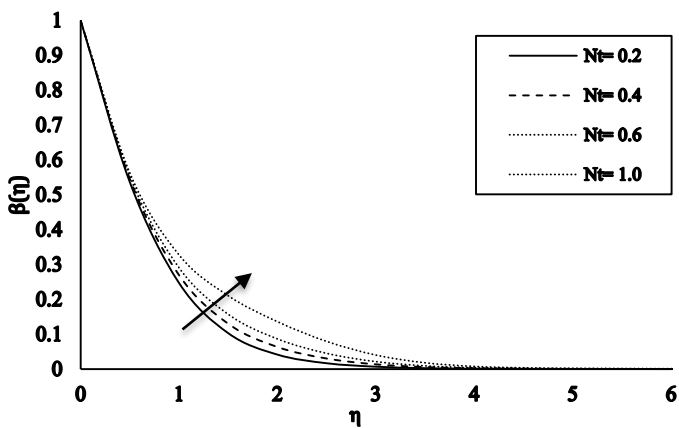


Figure. 13. Concentration profile vs Nt when $Nb = 0.5, Le = 2, Pr = M = 1, Bi = 0.5, \delta = 0.1, A = 0.4, Ec = 0.2$ and $\chi = 0.2$.

Chemical Reaction Parameter

Figure 14 illustrates the impact of the chemical reaction on the temperature profile for different values. It increases by increasing the

value of the chemical reaction parameter. Effect of χ on the concentration is shown in Figure 15. The concentration distribution increases with the increasing values of χ but a bit away from the surface it starts decreasing.

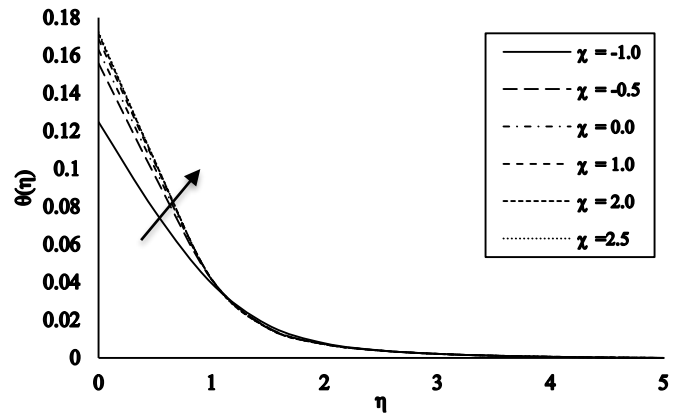


Figure. 14. Temperature profile vs χ when $Nb = Nt = 0.1, A = 0.4, Pr = 5, M = 1, Le = 2.0, Bi = 0.1, \gamma = 0.1, \delta = 0.2$ and $Ec = 0.2$.

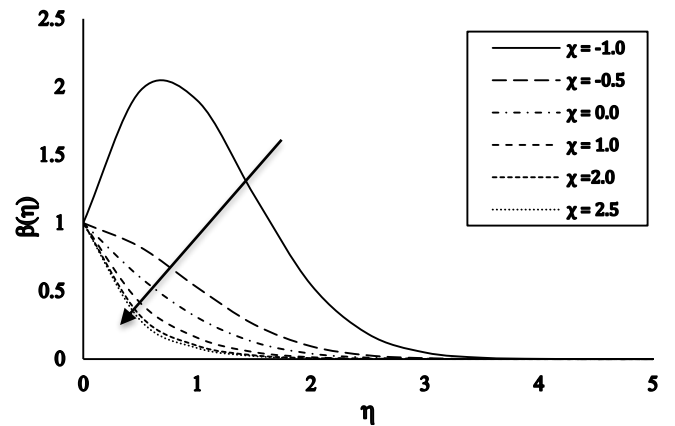


Figure. 15. Concentration profile vs χ when $Nb = Nt = 0.1, A = 0.4, Pr = 5, M = 1, Le = 2.0, Bi = 0.1, \gamma = 0.1, \delta = 0.2$ and $Ec = 0.2$.

Impact of slip parameter

The effect of slip parameter δ on the dimensionless velocity profile $f'(\eta)$ is presented in Figure 16. Increasing the values of the slip parameter δ reduces the velocity field and particular boundary thickness as depicted in Figure 16. Figure 17 illustrates the variations of slip parameter δ on the dimensionless energy profile $\theta(\eta)$. It is noted that $\theta(\eta)$ has direct relation with δ . Apparently, as δ mounts the lateral surface starts moving in y -direction, the energy profile $\theta(\eta)$ is increased.

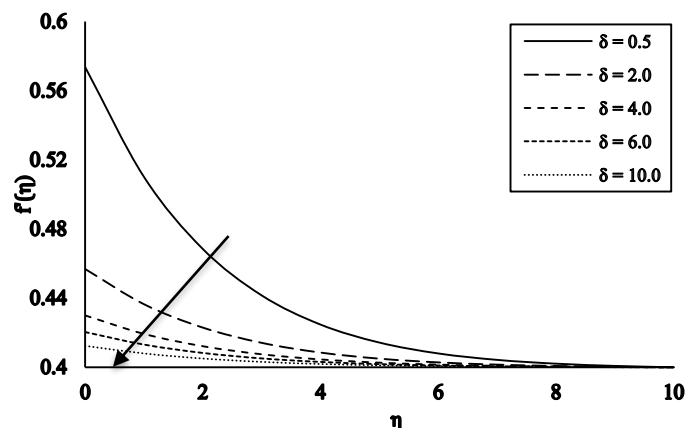


Figure 16. Velocity profile vs $\delta = 0.5, 2, 4, 6, 10$ when $Nt = Nb = 0.5, Le = 2, Pr = M = 1, Bi = 0.5, \gamma = 0.1, A = 0.4, Ec = 0.2, \chi = 0.2$.

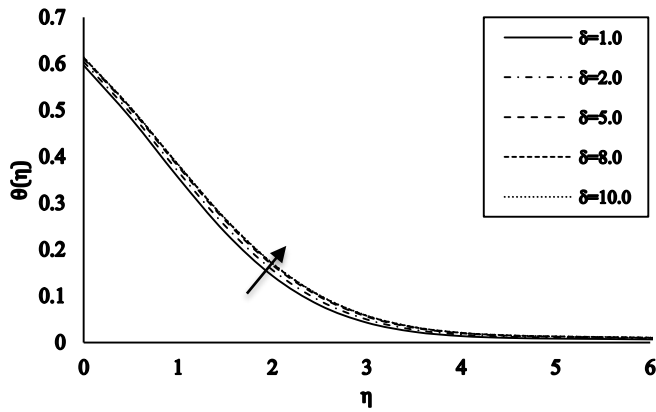


Figure 17. Temperature profile vs δ when $Nt = Nb = 0.5, Le = 2, Pr = M = 1, Bi = 0.5, \gamma = 0.1, A = 0.4, Ec = 0.2, \chi = 0.2$.

Impact of Eckert number on Nusselt number and Sherwood number

Figures 18 and 19 demonstrate the effect of Eckert number on local Nusselt number $-\theta'(0)$ and the local Sherwood number $-\beta'(0)$. From these figures, we observed that as the value of Ec increases, the local Nusselt number $-\theta'(0)$ at the surface decreases. However, it decreases as the value of Ec increases. Whereas the local Sherwood number $-\beta'(0)$ increases as the value of Ec increases.

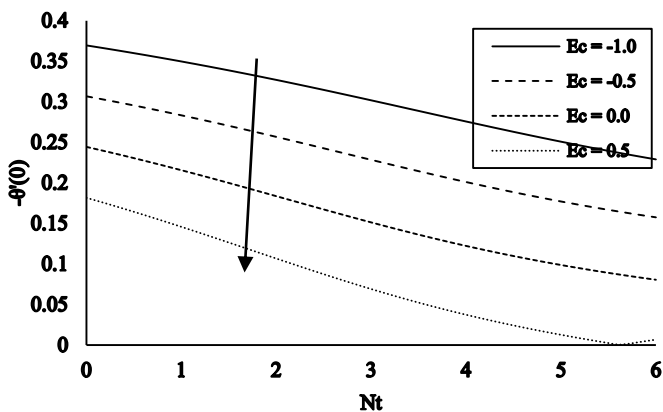


Figure 18. Graph of local Nusselt number vs (0) for different values of Ec when $Nb = 0.5, A = 0.4, Pr = 1, \delta = 0.1, M = 1, \gamma = 0.1, Le = 2$ and $\chi = 0.2$.

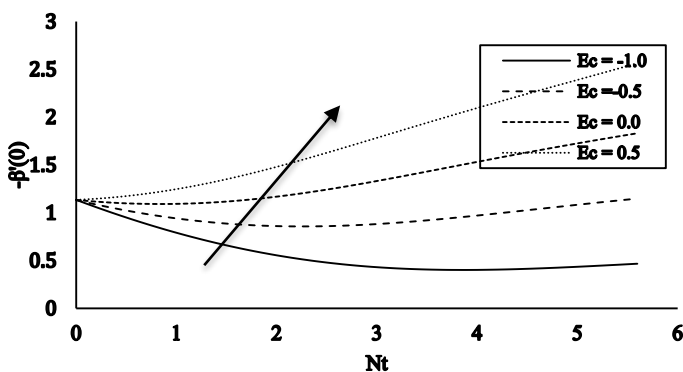


Figure 19. Graph of local Sherwood number $-\beta'(0)$ for different values of Ec when $Nb = 0.5, A = 0.4, Pr = 1, \delta = 0.1, M = 1, \gamma = 0.1, Le = 2$ and $\chi = 0.2$.

CONCLUSION

On the basis of the analysis of solution, the following conclusions have been drawn.

- Temperature and concentration are increased by enlarging thermophoresis parameter Nt .
- For larger values of Lewis number Le , Brownian motion Parameter Nb , and chemical reaction parameter χ , concentration field $\beta(\eta)$ shows decreasing behavior.
- The increase in thermal and concentration Biot number results in the increase of temperature and concentration profile.
- By increasing the thermophoresis parameter, this increases the concentration profile.
- The velocity profile increases by increasing the velocity ratio parameter A but the temperature and concentration profiles are decreased by increasing A .
- Energy profile $\theta(\eta)$ increases by enlarging Ec .
- Increasing the values of the slip parameter δ reduces the velocity field.

ACKNOWLEDGEMENT

The authors would like to thank Prof. Koneru S.R., Retired Professor, Department of Mathematics, IIT Bombay for his support throughout this research work.

REFERENCES

- [1] Carragher, P., Crane, L. (1982). Heat Transfer on Continuous Stretching Sheet, *ZAMM*, 10(62), 564-565.
- [2] Na, T. Y., and Pop, I. (1996). Unsteady flow past a stretching sheet, *Mechanical Research Communications*, 23, 413-422.
- [3] Pop, S. R. (2004). Radiation effect on the flow near the stagnation point of a stretching sheet, *Technische Mechanik*, 25, 100-106.
- [4] Jang, S. P., and Choi, S. U. S. (2007). Effects of various parameters on nanofluid thermal conductivity, *Journal of Heat Transfer*, 129, 617-623.
- [5] Kuznetsov, A. V., and Nield, D.A. (2009). The Cheng–Minkowycz problem for natural convective boundary-layer flow in a porous medium saturated by a nanofluid, *International Journal of Heat and Mass Transfer*, 52, 5792-5795.
- [6] Nield, D. A., and Kuznetsov, A.V. (2010). Natural convective boundary-layer flow of a nanofluid past a vertical plate, *International Journal of Thermal Sciences*, 49, 243-247.
- [7] Khan, W. A., and Pop, I. (2010). Boundary-layer flow of a nanofluid past a stretching sheet, *International Journal of Heat and Mass Transfer*, 53, 2477-2483.
- [8] Ibrahim, W., and Shankar, B. (2013). MHD boundary layer flow and heat transfer of a nanofluid past a permeable stretching sheet with velocity, thermal and solutal slip boundary conditions. *Computers & Fluids*, 75, 1–10.
- [9] Abo-Eldahab, E. M., and M. A. El Aziz, M. A. (2005). Viscous dissipation and Joule heating effects on MHD-free convection from a vertical plate with power-law variation in surface temperature in the presence of Hall and ion-slip currents, *Applied Mathematical Modelling*, 29(6), 579-595.
- [10] Sahoo, B. (2009). Effects of partial slip, viscous dissipation and Joule heating on von karman flow and heat transfer of an electrically conducting non-Newtonian fluid, *Communications in Nonlinear Science and Numerical Simulation*, 14(7), 2982-2998.
- [11] Sreenivasulu, P., Poornima, T., and Reddy, N. B. (2016). Thermal radiation effects on MHD boundary layer slip flow past a permeable exponential stretching sheet in the presence of Joule heating and viscous dissipation, *Journal of Applied Fluid Mechanics*, 9(1), 267-278.
- [12] Noghrehabadi, A., Pourrajab, R., and Ghalambaz, M. (2012). Effect of partial slip boundary condition on the flow and heat transfer of nanofluids past stretching sheet prescribed constant wall temperature. *International Journal of Thermal Sciences*, 54, 253-261.
- [13] Ibrahim, W., and Makinde, O. D. (2016). Magnetohydrodynamic stagnation point flow and heat transfer of Casson nanofluid past a stretching sheet with slip and convective boundary condition, *Journal Aerospace Engineering*, 29(2), 04015037(1-11).
- [14] Andersson, H. (2002). Slip flow past a stretching surface. *Acta Mechanica*, 158(1), 121–125.
- [15] Hayat, T., Qasim, M., and Mesloub, S. (2011). MHD flow and heat transfer over permeable stretching sheet with slip conditions. *International Journal Numerical Methods in Fluids*, 66(8), 963–975.